TRANSPORT
ISSN 1648-4142 / eISSN 1648-3480
2019 Volume 34 Issue 2: 250–259
https://doi.org/10.3846/transport.2019.9043

MODEL-BASED ASSESSMENT OF LONGITUDINAL DYNAMIC PERFORMANCE AND ENERGY CONSUMPTION OF HEAVY HAUL TRAIN ON LONG-STEEP DOWNGRADES

Jin SHI[1*], Shujing REN[2], Mengran ZHANG[3]

[1, 2]*School of Civil Engineering, Beijing Jiaotong University, China*
[3]*China Railway Engineering Consulting Group Co., Ltd., China*

Received 3 June 2017; revised 3 August 2017; accepted 15 November 2017

Abstract. Longitudinal dynamics performance and energy consumption of heavy haul train should be considered in the design of heavy haul railway profile of long-steep downgrades. A quantitative analytical tool is developed to assess the longitudinal dynamic performance and energy consumption of heavy haul trains with large axle loads on grades with different longitudinal profiles, including a longitudinal dynamic model of the train and a method of calculating the energy consumption during the operation of heavy haul train. The model is then preliminarily validated by the data of coupler force collected in two comprehensive tests. Finally, the proposed analytical tool is used to assess the designed longitudinal track profile of a long-deep downgrade segment of the central south heavy haul railway of Shanxi (China).

Keywords: heavy haul train, longitudinal dynamics, long-steep downgrades, cyclic braking, energy consumption.

Introduction

Heavy haul transportation is the main direction of development for railway freight transportation in China and the world. In recent years, heavy haul railways constructed in China need to pass through perilous mountainous areas, so tracks with steep grades are often applied to overcome the difference in terrain elevation. The operational modes, such as traction and braking, of heavy haul train on steep grades not only result in longitudinal, impulsive train motion, but also alter the operational energy consumption; therefore, in the design of longitudinal track profile, not only the engineering investment should be considered, but the influence of the longitudinal profile on the operation of heavy haul train should also be considered.

Air brake and the buffering model are essential in the longitudinal dynamics model to simulate the process of braking. Some researches have been done on the longitudinal dynamics for the reference. The paper by Murtaza (1993) have developed railway air brake simulation by using empirical equations and predicted theoretical brake models. Pugi *et al.* (2008) have proposed simulation models of the pneumatic plant of the International Union of Railways (UIC) railway brake including libraries of pneumatic submodels. A freight car air brake system simulation model based on airflow dynamics and function principle of the "120" control valve is established which shows good consistence with the experiment results (Wei, Lin 2009). Piechowiak (2009) created separate partial models with different levels of accuracy taking into account airwave phenomena. Various experimental studies were carried out on their own and other test stands to verify numerical models, determine the parameters and create relatively complete models of the rail brake system (Piechowiak 2010). The train air brake system mode was integrated into the train longitudinal dynamics study that focuses on the locomotive automatic brake valve and vehicle distribution valve model (Wei *et al.* 2017). The paper by Afshari *et al.* (2013) focused on the integration of a model of a train's air brake and a non-linear model of a train's dynamics.

Three types of wagon connection coupling systems including autocouplers with standard draft gears, autocouplers with draft gears with wedge unlocking features and the traditional drawhook buffer system were evaluated (Cole, Sun 2006). Paper by Wu *et al.* (2017) compared three types of draft gears with different damping mechanisms: friction, polymer and friction-polymer. The paper

*Corresponding author. E-mail: *jshi@bjtu.edu.cn*

by Wu *et al.* (2014a) reviewed current techniques in dynamics modelling of friction draft gears to provide a starting point that can be used to improve existing or develop new models to achieve more accurate force amplitude and pattern predictions. An advanced explicit dynamic modelling approach (Wu *et al.* 2015) with all components of the draft gear and their geometries considered for friction draft gears has been proposed and the conventional two-stage (loading and unloading) working process of the friction draft gear was detailed as a four-stage process.

According to the above method, some papers have integrated longitudinal dynamics model. The paper by Belforte *et al.* (2008) presented an analysis of heavy freight train dynamics and the proposed methodology combined a new numerical model designed for the longitudinal dynamics of the whole trainset. The paper by Pugi *et al.* (2011) describes a full model of the pneumatic plant and buffers and draw gears as well as a mechanical model that may be mono-dimensional or tri-dimensional for simulating and optimizing freight wagons composition rules. The longitudinal dynamics model of heavy-haul trains, air brake model and draft gear model used in the Longitudinal Train Dynamics (LTDs) were established (Chang *et al.* 2017). The paper by Wu *et al.* (2016) discusses numerical solvers, vehicle connection systems, air brake systems, wagon dumper systems and locomotives, resistance forces and gravitational components, vehicle in-train instabilities, and computing schemes.

Based on the LTDs, scholars proposed methods about energy consumption and how to reuse energy. A new technology named Train Dynamics and Energy Analyser/train Simulator (TDEAS) has been developed to perform detailed whole trip LTDs and energy analyses (Wu *et al.* 2014b). The paper by Sun *et al.* (2014) studied the energy used by heavy haul trains and the amount of energy that can be generated from dynamic braking of these trains using the CRE-LTS software package. Conti *et al.* (2015) proposed an innovative integrated procedure in the *Matlab Simulink* environment to optimise LTDs and traction and braking manoeuvres in terms of both energy and wear. The paper by Lebedevas *et al.* (2017) proposed the experimental and mathematical modelling increase the energy efficiency and reduce fuel consumption from diesel engines of locomotives via the main lines of the Lithuanian railway network.

However, a lack of research is noted in the existing literature on how the longitudinal profile of heavy haul railway affects the operational energy consumption and longitudinal dynamic behaviour of train. In order to provide a quantitative analytical tool for assessing the longitudinal dynamic performance and energy consumption of heavy haul trains with large axle loads on grades with different longitudinal profiles and improve the design of heavy haul railway, a longitudinal dynamic model of heavy haul train with large axle load is constructed based on the current engineering practice in China, and a method of calculating the energy consumption during the operation of heavy haul train is proposed. The model is then preliminarily validated by the data of coupler force measured in the comprehensive tests for heavy haul trains running on the Beijing–Guangzhou railway and the central south heavy haul railway of Shanxi, and the procedure is introduced of predicting the longitudinal dynamic performance and energy consumption of a train running under the conditions of uphill traction and downhill cyclic braking. Finally, the proposed model and procedure is used to assess the design of longitudinal track profile of a long-deep downgrade segment of the central south heavy haul railway of Shanxi.

1. The simulation models

1.1. Longitudinal dynamic model of heavy haul train

The model proposed in this paper adopts the HXD1 locomotive and the C96 vehicle with axle load of 30 t.

1.1.1. Kinetic equations

In studying the longitudinal dynamics of train, the lateral and vertical motions can be neglected, and only the longitudinal degree of freedom is considered. The train is assumed to be a discrete mass system consisting of a plurality of rigid bodies (locomotives and vehicles) connected by elastic elements (coupler buffer device), as shown in Figure 1.

According to the D'Alembert's principle, the differential equations governing the motion of the train are established as follows:

$$m_i \cdot \ddot{x}_i = S_i - S_{i+1} + \omega_{0i} + F_1 + B_i + D_1 + P_i, \quad (1)$$

where:

$S_i = S_i\left(\dot{q}_i, q_i\right)$;

$\omega_{0i} = \omega_{0i}\left(\dot{x}_i, x_i\right)$;

$F_1 = F_1\left(\dot{x}_1\right)$;

$B_i = B_i\left(\dot{x}_i, t\right)$;

$D_1 = D_1\left(\dot{x}_1, t\right)$;

$P_i = P_i\left(x_i\right)$,

where: i is the grouping number of vehicles; m_i is the mass

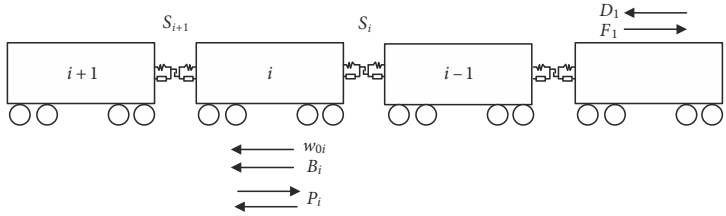

Figure 1. Discrete-mass system model of the train

of locomotive or vehicle [t]; S_i and m_i S_{i+1} are the maximum longitudinal force (coupler force) between the i-th and $(i + 1)$-th vehicles [kN]; ω_{0i} is the basic resistance of locomotive or vehicle [kN]; P_i is gradient resistance [kN]; F_1 is the traction force [kN]; B_i and D_1 are the air braking force [kN] and locomotive electric braking force [kN], respectively, and they cannot coexist with F_i; x_i, $\dot{x}_i$ and $\ddot{x}_i$ are the absolute displacement, velocity, and acceleration of the locomotive or vehicle [m], [m/s] and [m/s^2], respectively; q_i and $\dot{q}_i$ are the relative displacement and velocity between two adjacent vehicles [m] and [m/s], respectively; t is the braking time [s].

1.1.2. Characteristics of air brake system

In the proposed vehicle model, the 120-type brake is used. In the simulation of the air brake system, 4 key parameters are required: the brake shoe pressure K, air pressure in the brake cylinder p_z, number of brake shoes per vehicle n_k, and frictional coefficient of brake shoe φ_k. The braking force acting on each vehicle can be expressed as:

$$B = K \cdot \varphi_k \cdot n_k, \tag{2}$$

where: B is the braking force for each vehicle [kN].

The brake shoe pressure of each brake shoe K can be expressed as:

$$K = \frac{\frac{\pi}{4} \cdot d_z^2 \cdot p_z \cdot \eta_z \cdot \gamma_z \cdot n_z}{n_k \cdot 10^6}, \tag{3}$$

where: π is the circumference diameter ratio, which is approximated as 3.1416; d_z is the radius of brake cylinder [mm]; p_z is the air pressure in the brake cylinder [kPa]; η_z is the calculated transmission efficiency of the basic braking device; γ_z is the braking leverage ratio; n_z is the number of brake cylinders; n_k is the number of brake shoes.

For the simulated HXD1 locomotive, the diameter of brake cylinder is 178 mm, the transmission efficiency is 0.87, the braking leverage ratio is 2.85, and the number of brake cylinders is 16. In each brake, 2 high-friction synthetic brake shoes are installed. For the C96 vehicle, the diameter of brake cylinder is 254 mm, the transmission efficiency is 0.9, the braking leverage ratio is 4.85, and the number of brake cylinders is 2.

Pressure reduction of 140 kPa in the train brake pipe is used in regular train braking, and smaller pressure reduction of 50 kPa is used in cyclic braking. Figures 2a and 2b show the variation of pressure in the brake cylinder corresponding to the amount of pressure reduction in the train brake pipe.

In this paper, high-friction composite brake shoe is adopted in the model, and the frictional coefficient between the brake shoe and brake pad is:

$$\varphi_k = 0.41 \cdot \frac{K + 200}{4 \cdot K + 200} \cdot \frac{v + 150}{2 \cdot v + 150}, \tag{4}$$

where: K is the pressure [kN] of brake shoe (or brake pad) acting on the wheel (or brake disc) [kN]; v is the running speed of the train during braking [km/h].

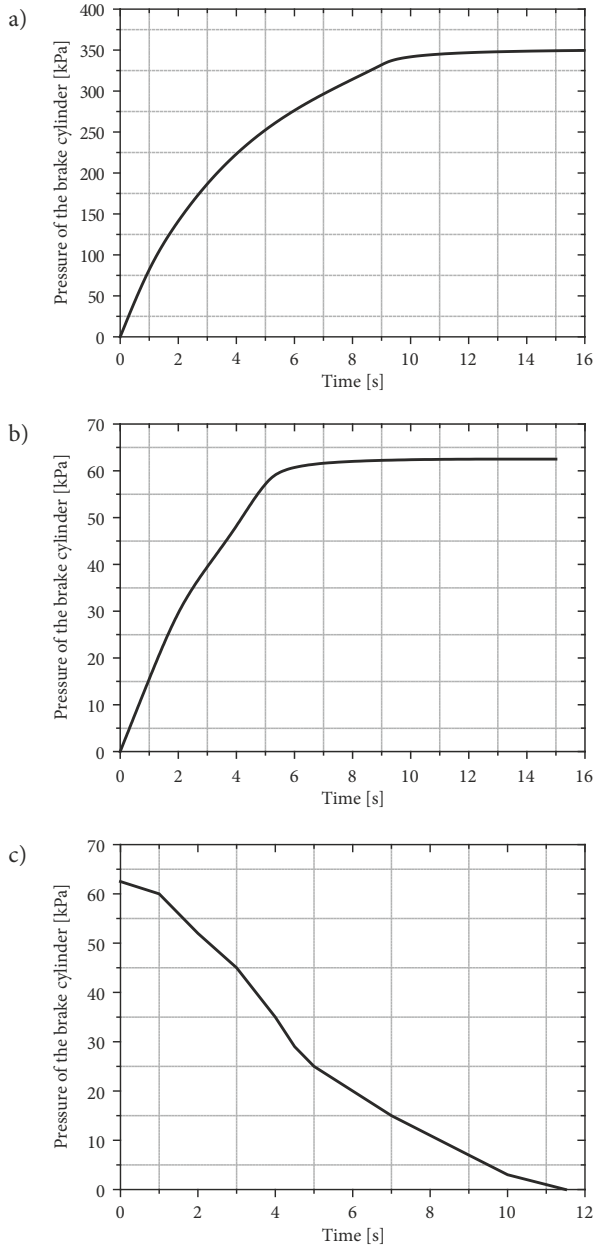

Figure 2. Pressure variation in the brake cylinder corresponding: a – 140 kPa pressure reduction used in regular train braking; b – 50 kPa pressure reduction used in cyclic braking; c – release characteristic of the train in cyclic braking

1.1.3. Characteristics of coupler buffer device

In consideration of the characteristics of heavy haul train, the No 17 chain-fixed coupler and the MT-2 type buffer are adopted in the model.

Figure 3 shows the characteristic curve of resistant force vs displacement for the MT-2 type buffer after linear fitting. The dynamic characteristic curve of buffer force-displacement can be determined by the envelope of multiple results obtained in the drop hammer tests at different heights. The characteristic curve takes into account factors such as the coupler clearance and the initial pressure of the buffer, and can be used to describe the loading and unloading processes. The loading impedance character-

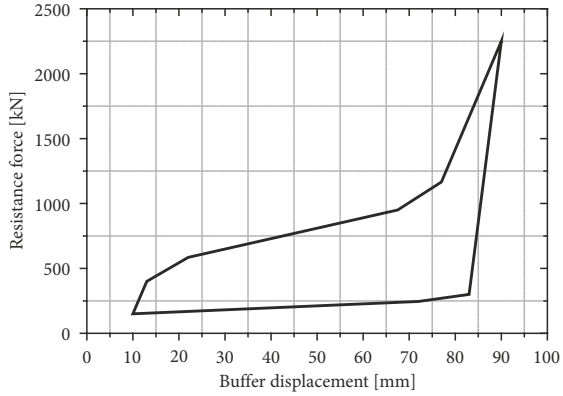

Figure 3. Dynamic model of the MT-2 type buffer – resistance force vs buffer displacement

istic curve is not consistent with the unloading impedance characteristic curve in this figure, demonstrating the properties of nonlinear hysteresis.

1.1.4. Track resistance model

The unit basic resistance of a running HXD1 locomotive is calculated by (Wu *et al.* 2016):

$$w_0' = 1.4 + 0.0038 \cdot v + 0.0003 \cdot v^2, \tag{5}$$

for the C96 freight car, the formula is:

$$w_0'' = 0.92 + 0.0048 \cdot v + 0.000126 \cdot v^2, \tag{6}$$

where: w_0' is the unit basic resistance of the running locomotive [N/kN]; w_0'' is the unit basic resistance of the running freight car [N/kN].

When the length of the train is less than or equal to the length of the curve, the unit curve additional resistance of the freight train is:

$$\omega_r = \frac{600}{R} \cdot g, \tag{7}$$

or the unit curve additional resistance is:

$$\omega_r = \frac{600}{R} \cdot \frac{l_r}{l_l} \cdot g, \tag{8}$$

where: ω_r is the curve additional resistance [N/t]; R is the curve radius [m]; g is the gravitational acceleration [m/s^2]; l_r is the length of the curve [m]; l_l is the length of the train [m].

1.2. Energy composition and calculation method

In the operation of heavy haul train, 8 different forms of energy are involved:

- locomotive tractive energy E_T;
- locomotive braking energy consumption E_D;
- basic resistive energy consumption E_p;
- curve induced additional resistance energy consumption E_C;
- air braking energy consumption E_A;
- gravitational potential energy E_G;
- kinetic energy of the train E_K;
- coupler-buffer device energy consumption E_{DG}.

The law of energy conservation is observed in the running of heavy haul train, i.e.:

$$E_T = \left(E_{K2} - E_{K1}\right) + \left(E_{G2} - E_{G1}\right) + E_D + E_P + E_C + E_A + E_{DG}. \tag{9}$$

According to ref (Wu *et al.* 2014a, 2014b), the energy consumed by the coupler-buffer device constitutes a small proportion of the total energy consumption ($2.79 \cdot 10^{-5}$%), so it can be ignored in the calculation of energy consumption. The curve-induced additional resistance is small when the train is running, so it is not considered either. Therefore, the forms of energy considered in this paper only include the locomotive tractive energy E_T, locomotive braking energy consumption E_D, basic resistive energy consumption E_p, air braking energy consumption E_A, gravitational potential energy E_G, and kinetic energy of the train E_K.

The first five forms of energy are calculated according to the work done by the force. Assume that the internal force is constant at each calculation step, and then the formula is:

$$E_A = \sum_{i=1}^{m} \sum_{j=1}^{n} f_{ij} \cdot \Delta s_{ij}, \tag{10}$$

where: m is the total number of locomotive and vehicles; n is the total number of calculation steps; f_{ij} is the magnitude of internal force at a certain calculation step (median); Δs_{ij} is the displacement deviation corresponding to each calculation step.

The kinetic energy can be calculated by:

$$E = \sum_{i=1}^{n} \frac{m_i \cdot V_i^2}{2}, \tag{11}$$

where: m_i is the mass of the i-th vehicle; V_i is the velocity of the i-th vehicle.

The final formula calculating the energy consumption is:

$$E_T = \left(E_{K2} - E_{K1}\right) + \left(E_{G2} - E_{G1}\right) + E_D + E_P + E_A. \tag{12}$$

1.3. Model validation

The proposed longitudinal dynamic model is validated by comparison of the coupler force computed with the proposed model and the results measured in the comprehensive test for heavy haul train on the Beijing–Guangzhou railway and the central south heavy haul railway of Shanxi. The train tested on the Beijing–Guangzhou railway is composed of 12 C64(H) – type freight cars, 12 C70 or C70E – type freight cars, and 26 27-ton axle-load vehicles including flatcar, boxcar and tank car. This train is 753 m long, and is towed by a single locomotive providing 5000-ton traction force. The coupler force of the 15-th bit is collected on site. The train tested on the central south heavy haul railway of Shanxi is composed of 100 C96-type freight cars, and the 12000-ton traction force is provided by two locomotives in the front and two at the end.

Table 1. Measured and simulated results

Measurement location	Coupler location	Measured result [kN]	Simulated result [kN]	Working condition
The central south heavy haul railway of Shanxi (flat, straight track)	84	1525.2	1566.1	Emergency initial braking speed 70 km/h
	100	–823.9	–866.1	
The Beijing–Guangzhou railway (straight downgrade with –0.5‰ slope gradient)	15	350.8	373.8	Regular initial braking speed 8.4 km/h
	15	321.9	330.1	Regular initial braking speed 5.8 km/h

The coupler forces of the 84-th and 100-th bit are collected. Table 1 shows the comparison between the measured data and simulation results. The results calculated with the model are in good agreement with the test results, and the model is validated preliminarily.

2. Results of heavy haul train running under downhill, cyclic braking conditions

2.1. Calculated working conditions

The proposed model is used to analyse the longitudinal dynamic performance and energy consumption of a 10000-ton heavy haul train towed by two HXD1-type head locomotives with the "1+1" form of composition. The grouping number of the C96-type freight car (with axle load of 30 t) is 84; the initial braking speed is 70 km/h in the course of cyclic braking, the initial release speed is 40 km/h, and the maximum dynamic braking force of a single locomotive is 461 kN. The train is applied the maximum dynamic braking force when it is running under long-steep downgrades for the safety and the force acts on the locomotive.

The train is running on a downgrade with length of 10 km and gradient of 1…13‰. According to the mechanical analysis, when the gradient is less than 5‰, the exertion of locomotive electric braking force will cause the train to slow down; therefore, only when the gradient is greater than 5‰, the locomotive electric braking provided by a single locomotive should be applied.

2.2. Predicted longitudinal dynamic performance

2.2.1. Braking time and release time

In the course of downhill cyclic braking, the operation status of heavy haul train is decided by the gradient of the longitudinal track profile and the braking performance of the train. The evaluation factors are the braking time and the release time (the release time is also called the time available for recharging) during cyclic braking. Too short recharging time for the train (less than 2 min) will lead to insufficient recharging and affect the braking performance in the next cycle.

Table 2 shows the calculated braking time and release time during the cyclic braking of this heavy haul train for different slope gradients. With the increase of slope gradient, the braking time increases and the release time decreases rapidly; the exertion of locomotive electric braking force leads to salient increase in the release time but has small effect on the braking time. When the slope gradient is small, the release time is long, and the recharging requirements can be satisfied without the exertion of locomotive electric braking force. When the slope gradient is larger (greater than 10‰), the release time is almost close to 2 min, so it is more secure to activate the locomotive electric braking simultaneously provided by two locomotives on continuous slopes with large gradients.

2.2.2. Coupler force and acceleration

In order to analyse the variation of longitudinal dynamic performance on downgrades with different gradients during cyclic braking, the coupler force and acceleration at different locations on the train (head vehicle, 20, 40, 60 and 80% total train length from the head, tail vehicle) running on downgrades with 1, 5, 8 and 13‰ gradients are analysed in the course of cyclic braking.

Figure 4 shows the longitudinal dynamic performance of the train on a downgrade with 13‰ gradient. During a cycle, the coupler force and acceleration will fluctuate when the braking or release starts, and then reach their maximum values. With the completion of brake wave and release wave transmission, the fluctuations of the coupler force and acceleration tend to be stable. The coupler force decreases with the backward shift of coupler location, and owing to the existence of locomotive electric braking force, the train coupler is always in a state of compression. The coupler force of the head vehicle is always above

Table 2. Calculated results during cyclic braking of heavy haul train running on downgrades with different slope gradients

Slope gradient [‰]	0	–1	–2	–3	–4	–5	–6
Braking time	1 min 12 s	1 min 18 s	1 min 25 s	1 min 33 s	1 min 44 s	1 min 56 s	1 min 22 s
Release time	–	–	12 min 32 s	6 min 56 s	4 min 48 s	3 min 40 s	16 min 47 s
Slope gradient [‰]	–7	–8	–9	–10	–11	–12	–13
Braking time	1 min 30 s	1 min 40 s	1 min 52 s	2 min 7 s	2 min 26 s	2 min 54 s	3 min 6 s
Release time	8 min 3 s	5 min 21 s	3 min 57 s	3 min 10 s	2 min 37 s	2 min 15 s	2 min 1 s

400 kN, which is close to the locomotive electric braking force, but the coupler force of tail vehicle is very small, approximately 0.

Table 3 gives the maximum coupler tensile and compressive forces of the train in downhill cyclic braking. In the entire cyclic braking, the coupler forces are much smaller than the calibration standard required for the Class-I special vehicles under the first working condition, 2000 kN tensile force and 2250 kN compression force. The accelerations are less than 10 m/s^2 and all within the safe limit.

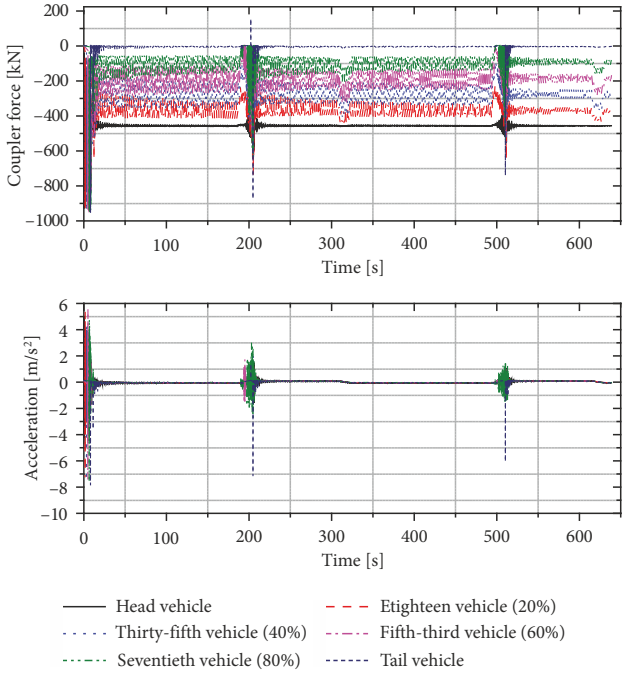

Figure 4. Coupler force and acceleration when the slope gradient is –13‰

Table 3. Longitudinal dynamic performance of heavy haul train during cyclic braking

Slope gradient [‰]	–1	–5	–8	–13
Maximum coupler force [kN]	–881.12	–901.04	–958.51	–960.96
Maximum coupler force [kN]	873.08	870.82	321.4	153.51
Maximum positive acceleration [m/s^2]	7.15	7.18	6.04	5.53
Maximum negative acceleration [m/s^2]	–7.43	–7.59	–7.97	–7.67

2.3. Predicted energy consumption

Figure 5 shows the variation of energy consumption of the train running on downgrades with different slope gradients. The basic resistance energy consumption and locomotive braking energy consumption do not vary much. With the increase of slope gradient, the energy consumption of air braking tends to increase, and when the

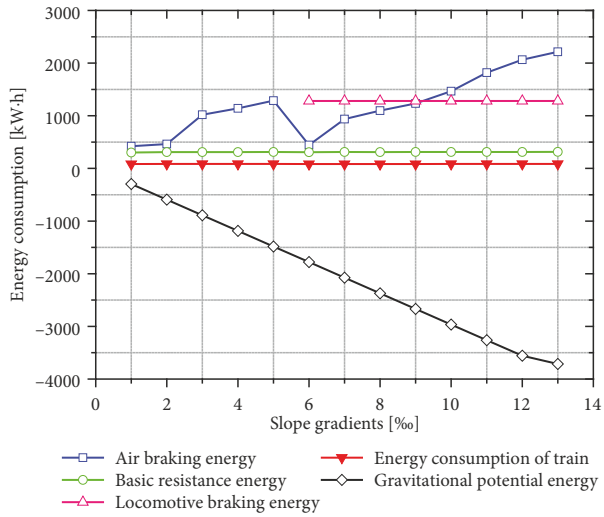

Figure 5. Energy consumption of train for different slope gradients

gradient is greater than 6‰, in order to ensure sufficient recharging, the locomotive braking force is applied, and then the braking distance of the train is reduced and the energy consumption of air braking is also greatly reduced. When the slope gradient is small, activation of the locomotive braking force can reduce the energy consumption of air braking; however, with the increase of slope gradient, the energy consumption of air braking will increase rapidly. In the course of cyclic braking of heavy haul train running downhill, the gravity does positive work, and the variation of gravitational potential energy can be used as a source of energy input to the train system, so the total energy consumption of the train is very small. With the increase of slope gradient, the braking energy consumption will increase, and the change of gravitational potential energy will increase accordingly; however, the basic resistance energy consumption and kinetic energy variation of the running train have not changed, so the total energy consumption is approximately constant.

Figure 6 shows the composition of energy consumption during cyclic braking of the training running on downgrades with different slope gradients. The braking energy consumption (including the air braking energy consumption and locomotive braking energy consumption) always constitutes the largest proportion of energy consumption, accounting for more than 50%. When the slope gradient is small, the air braking energy consumption constitutes a larger proportion; after the locomotive braking force is applied, the locomotive braking energy consumption becomes the major part, and the proportion of the energy consumed by air braking is significantly reduced. With the increase of slope gradient, the braking distance increases, and the proportion of energy consumed by air braking increases and becomes the major component of the total energy consumption, while the proportion of basic resistance energy consumption decreases rapidly with the increase of slope gradient.

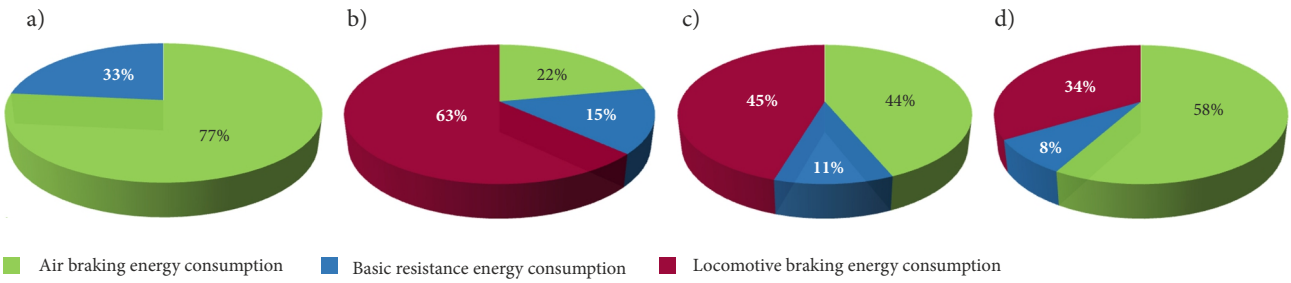

Figure 6. Composition of energy consumption of train during cyclic braking for different slope gradients: a – 3‰; b – 6‰; c – 9‰; d – 13‰

3. Case study of the South Changzi station–South Shuizhi station segment

3.1. Engineering survey

The most difficult segment in the design of the central south heavy haul railway of Shanxi is the Huguan–South Shuizhi long-steep downgrade more than 100 km long and with the maximum gradient of 13‰, as shown in Table 4. In order to include all the operating conditions of a running train, the longitudinal dynamics is simulated of a heavy haul train running on a 155 km long railway in the South Changzi station–South Shuizhi station segment.

The slope gradient and longitudinal profile of this segment are shown in Table 4 and Figure 7, respectively. A heavy haul train departs from the South Changzi station (elevation 948.8 m), goes through an upgrade about 45 km long, and reaches the highest point in this segment – the Huguan station (elevation 1020.19 m). The train then enters into the long-steep downgrade (about 100 km long) in the Huguan station–South Shuizhi station segment and cyclic braking is applied. Finally, the train is decelerated by full braking to 0 m/s and stops at the South Shuizhi station (elevation 123.77 m). The whole-course elevation difference is up to 896.42 m.

Table 4. Slope gradients in the South Changzi station–South Shuizhi station segment

Mileage at varied slope gradient	Designed shoulder elevation [m]	Designed slope gradient [‰]	Annotations
D1K484+400.00	948.80	0.00	The South Changzi station
DK494+500.00	991.23	5.00	
DK495+150.00	994.48	–3.00	
DK496+000.00	988.73	–13.00	
DK503+400.00	995.27	5.20	
DK523+700.00	1021.19	–4.00	
DK525+600.00	1020.09	2.10	
DK526+700.00	1020.19	–1.00	The Huguan station
DK529+500.00	1016.04	–13.00	
DK537+500.00	952.57	3.50	
DK543+100.00	908.11	–13.00	
DK597+500.00	353.97	6.00	
D1K601+050.00	357.87	–9.00	
D1K602+330.00	344.81	1.00	
D1K610+100.00	324.81	–13.00	
DK615+930.00	279.14	3.00	
DK617+600.00	281.45	–13.00	
DK631+750.00	123.77	–1.00	The South Shuizhi station

3.2. Predicted longitudinal dynamic performance

The simulated train has the same formation as in Section 3. When running in the South Zhangzi station–South Shuizhi station segment, the train will undergo four stages: "starting → constant velocity → cycle braking → full braking". Figure 8 shows the time history curve of the locomotive speed. In the whole course of train operation, the train speed is between 35…75 km/h and can meet the speed limit.

3.2.1. Braking time and release time

Table 5 shows the calculated results for the braking and releasing processes. A total of 14 complete cycles of braking are applied. The braking time is less than 3 min, and the release time is above 2 min, so the train has good braking and release performance, and the recharging requirement can be satisfied in this segment.

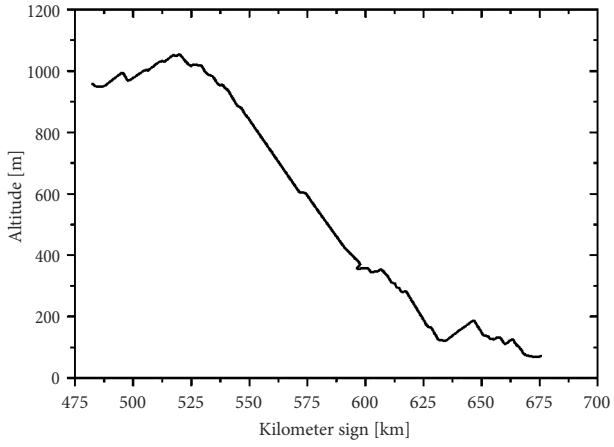

Figure 7. Contracted longitudinal profile of the South Changzi station–South Shuizhi station segment

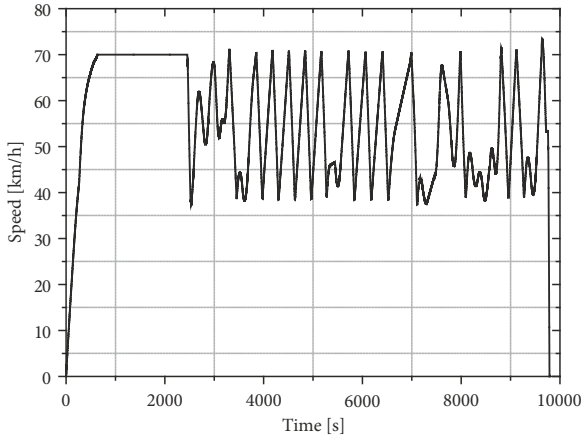

Figure 8. Time history of velocity in the South Changzi station–South Shuizhi station segment

Table 5. Simulated results for cyclic braking

Number of cycles of braking	Braking time	Time available for recharging	Initial braking speed [km/h]	Initial release speed [km/h]
1	1 min 1 s	13 min 3 s	70	40
2	2 min 28 s	6 min 37 s	70	40
3	2 min 3 s	3 min 26 s	70	40
4	2 min	3 min 32 s	70	40
5	2 min 1 s	3 min 28 s	70	40
6	2 min 2 s	3 min 25 s	70	40
7	1 min 47 s	7 min 24 s	70	40
8	1 min 58 s	3 min 47 s	70	40
9	1 min 54 s	3 min 50 s	70	40
10	1 min 54 s	7 min 49 s	70	40
11	1 min 54 s	14 min 41 s	70	40
12	1 min 48 s	11 min 56 s	70	40
13	2 min 27 s	2 min 41 s	70	40
14	2 min 37 s	6 min 1 s	70	40

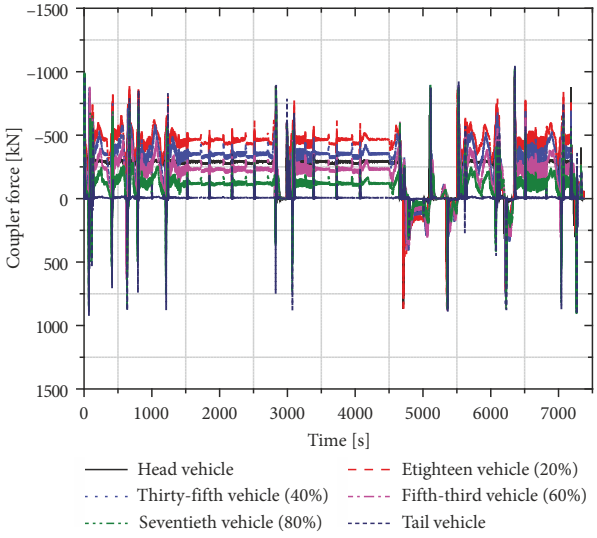

Figure 9. Time history of coupler force in the course of cyclic braking

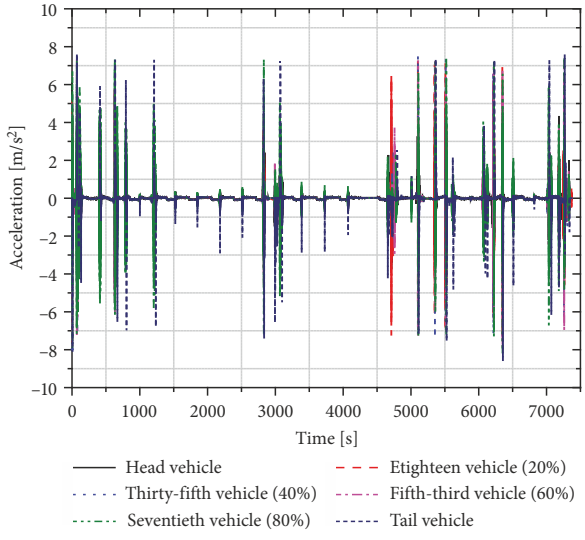

Figure 10. Time history of acceleration in the course of cyclic braking

3.2.2. Coupler force and acceleration

In order to analyse the coupler force and acceleration at different locations of the train, the coupler force and acceleration are analysed at different locations of the train (head vehicle, 20, 40, 60 and 80% total train length from the head, tail vehicle). The calculated results are shown in Figures 9 and 10. The coupler force and acceleration display a wide range of fluctuations when the braking and the release start. With the backward shift of coupler location, the coupler force gradually decreases and the coupler force at the end of the train is very small, close to 0. The maximum coupler tensile force is 921.65 kN, the maximum coupler compressive force is 1039.64 kN, the maximum positive acceleration is 7.63 m/s^2, and the maximum negative acceleration is –8.59 m/s^2. The couple tensile and compressive forces are far less than the required coupler calibration standards for the Class-I special vehicles under the first working condition: 2000 kN and 2250 kN, respectively, and the acceleration is less than the recommended level of 10 m/s^2 according to the safety control standard.

3.3. Predicted operational energy consumption

In the South Changzi station–South Shuizhi station segment, the energy source is the gravitational potential energy and locomotive traction energy, and the energy is mainly consumed by air braking, locomotive braking, and the basic resistance. Figure 11 shows the time history of energy consumption in the course of cyclic braking. The kinetic energy has the same trend of variation as the speed shown in Figure 8. The basic resistance energy consumption, air braking energy consumption and locomotive braking energy consumption continue to increase with time, but the basic resistance energy consumption is far less than the latter two forms of energy consumption

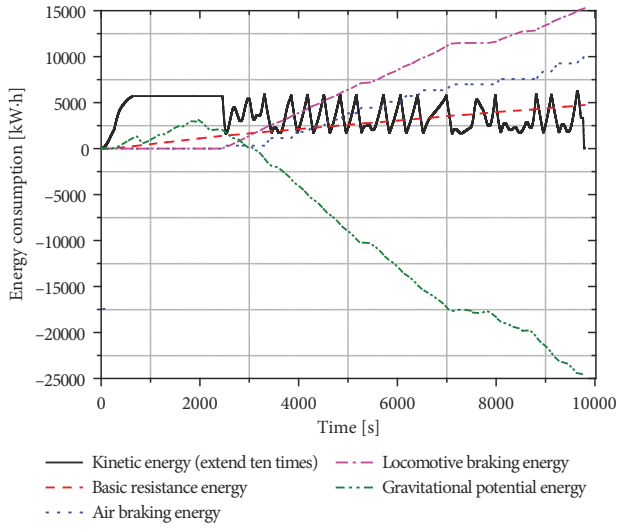

Figure 11. Time history of energy consumption in the course of cyclic braking

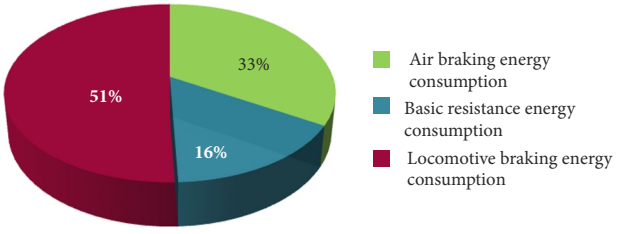

Figure 12. Composition of energy consumption in the course of cyclic braking

(also called the braking energy consumption). The gravitational potential energy first increases and then decreases, and shows a generally decreasing trend, because the segment profile is first upgrade and then downgrade, and the downgrade is the dominant part.

Figure 12 shows the composition of energy consumption in the same course. Because of the dominant long-steep downgrade in the segment, the major component is the braking energy consumption, accounting for more than 80% of the total energy consumption. The locomotive braking force exists in the entire braking process, so the locomotive braking energy consumption accounts for more than 50% of the total energy consumption, while the basic resistance energy consumption accounts for only 16% of the total energy consumption.

Conclusions

In this paper, a dynamic model is proposed to predict the longitudinal dynamic performance of a heavy haul train running on long-steep downgrades, and based on the model, methods of calculating the energy consumption are also proposed. The following conclusions are drawn:

1) To ensure sufficient time for recharging under the condition of downhill cyclic braking, electro-pneumatic blended braking is required. With the increase of slope gradient, the braking time increases and the release time decreases. When the slope gradient is greater than 10‰, the locomotive braking force provided by one locomotive will lead to almost 2 min release time;
2) The gravitational potential energy is the main energy source for heavy haul trains running on long-steep downgrades, and the total energy consumption of the train is far less than the locomotive traction energy consumption in the course of uphill traction; in the course of cyclic braking, the braking energy consumption always accounts for a large proportion of the total energy consumption (more than 50%);
3) The model is used to simulate a total of 14 full cycles of braking on the long-steep downgrade in the South Changzi station–South Shuizhi station segment in central south heavy haul railway of Shanxi. The results show that the braking time is less than 3 min and the release time is longer than 2 min; such good braking performance can satisfy the recharging requirements. When a train is running in this segment, the maximum coupler tensile force will be 921.65 kN, and the maximum coupler compressive force will be 1039.64 kN, far less than the coupler calibration standards required for the Class-I special vehicles under the first working condition: 2000 and 2250 kN, respectively. The total energy consumption in this segment is 5614.22 kWh, and the braking energy consumption accounts for more than 80% of the total energy consumption.

Acknowledgements

This work was supported by the National Natural Science Foundation of China under Grant [number 51578054].

References

Afshari, A.; Specchia, S.; Shabana, A. A.; Caldwell, N. 2013. A train air brake force model: car control unit and numerical results, *Proceedings of the Institution of Mechanical Engineers, Part F: Journal of Rail and Rapid Transit* 227(1): 38–55. https://doi.org/10.1177/0954409712447231

Belforte, P.; Cheli, F.; Diana, G.; Melzi, S. 2008. Numerical and experimental approach for the evaluation of severe longitudinal dynamics of heavy freight trains, *Vehicle System Dynamics: International Journal of Vehicle Mechanics and Mobility* 46: 937–955. https://doi.org/10.1080/00423110802037180

Chang, C.; Guo, G.; Wang, J.; Ma, Y. 2017. Study on longitudinal force simulation of heavy-haul train, *Vehicle System Dynamics: International Journal of Vehicle Mechanics and Mobility* 55(4): 571–582. https://doi.org/10.1080/00423114.2016.1269183

Cole, C.; Sun, Y. Q. 2006. Simulated comparisons of wagon coupler systems in heavy haul trains, *Proceedings of the Institution of Mechanical Engineers, Part F: Journal of Rail and Rapid Transit* 220(3): 247–256. https://doi.org/10.1243/09544097JRRT35

Conti, R.; Galardi, E.; Meli, E.; Nocciolini, D.; Pugi, L.; Rindi, A. 2015. Energy and wear optimisation of train longitudinal dynamics and of traction and braking systems, *Vehicle System*

Dynamics: International Journal of Vehicle Mechanics and Mobility 53(5): 651–671. https://doi.org/10.1080/00423114.2014.990466

Lebedevas, S.; Dailydka, S.; Jastremskas, V.; Rapalis, P. 2017. Research of energy efficiency and reduction of environmental pollution in freight rail transportation, *Transport* 32(3): 291–301. https://doi.org/10.3846/16484142.2016.1230888

Murtaza, M. A. 1993. Railway air brake simulation: an empirical approach, *Proceedings of the Institution of Mechanical Engineers, Part F: Journal of Rail and Rapid Transit* 207(1): 51–56. https://doi.org/10.1243/PIME_PROC_1993_207_226_02

Piechowiak, T. 2009. Pneumatic train brake simulation method, *Vehicle System Dynamics: International Journal of Vehicle Mechanics and Mobility* 47(12): 1473–1492. https://doi.org/10.1080/00423110802600946

Piechowiak, T. 2010. Verification of pneumatic railway brake models, *Vehicle System Dynamics: International Journal of Vehicle Mechanics and Mobility* 48(3): 283–299. https://doi.org/10.1080/00423110902780622

Pugi, L.; Palazzolo, A.; Fioravanti, D. 2008. Simulation of railway brake plants: an application to SAADKMS freight wagons, *Proceedings of the Institution of Mechanical Engineers, Part F: Journal of Rail and Rapid Transit* 222(4): 321–329. https://doi.org/10.1243/09544097JRRT118

Pugi, L.; Rindi, A.; Ercole, A. G.; Palazzolo, A.; Auciello, J.; Fioravanti, D.; Ignesti, M. 2011. Preliminary studies concerning the application of different braking arrangements on Italian freight trains, *Vehicle System Dynamics: International Journal of Vehicle Mechanics and Mobility* 49(8): 1339–1365. https://doi.org/10.1080/00423114.2010.505291

Sun, Y.; Cole, C.; Spiryagin, M.; Godber, T.; Hames, S.; Rasul, M. 2014. Longitudinal heavy haul train simulations and energy analysis for typical Australian track routes, *Proceedings of the Institution of Mechanical Engineers, Part F: Journal of Rail and Rapid Transit* 228(4): 355–366. https://doi.org/10.1177/0954409713476225

Wei, W.; Hu, Y.; Wu, Q.; Zhao, X.; Zhang, J.; Zhang, Y. 2017. An air brake model for longitudinal train dynamics studies, *Vehicle System Dynamics: International Journal of Vehicle Mechanics and Mobility* 55(4): 517–533. https://doi.org/10.1080/00423114.2016.1254261

Wei, W.; Lin, Y. 2009. Simulation of a freight train brake system with 120 valves, *Proceedings of the Institution of Mechanical Engineers, Part F: Journal of Rail and Rapid Transit* 223(1): 85–92. https://doi.org/10.1243/09544097JRRT119

Wu, Q.; Cole, C.; Luo, S.; Spiryagin, M. 2014a. A review of dynamics modelling of friction draft gear, *Vehicle System Dynamics: International Journal of Vehicle Mechanics and Mobility* 52(6): 733–758. https://doi.org/10.1080/00423114.2014.894199

Wu, Q.; Luo, S.; Cole, C. 2014b. Longitudinal dynamics and energy analysis for heavy haul trains, *Journal of Modern Transportation* 22(3): 127–136. https://doi.org/10.1007/s40534-014-0055-x

Wu, Q.; Luo, S.; Qu, T.; Yang, X. 2017. Comparisons of draft gear damping mechanisms, *Vehicle System Dynamics: International Journal of Vehicle Mechanics and Mobility* 55(4): 501–516. https://doi.org/10.1080/00423114.2016.1252049

Wu, Q.; Spiryagin, M.; Cole, C. 2015. Advanced dynamic modelling for friction draft gears, *Vehicle System Dynamics: International Journal of Vehicle Mechanics and Mobility* 53(4): 475–492. https://doi.org/10.1080/00423114.2014.1002504

Wu, Q.; Spiryagin, M.; Cole, C. 2016. Longitudinal train dynamics: an overview, *Vehicle System Dynamics: International Journal of Vehicle Mechanics and Mobility* 54(12): 1688–1714. https://doi.org/10.1080/00423114.2016.1228988